Designing a thermodynamically stable and intrinsically ductile refractory alloy

Sufyan M. Shaikh¹, B. S. Murty^{1, 2}, and Satyesh K. Yadav^{*1,3}

 ¹Department of Metallurgical and Materials Engineering, Indian Institute of Technology Madras, Chennai, 600036, Tamil Nadu, India
 ²Materials Science & Metallurgical Engineering, Indian Institute of Technology Hyderabad, Kandi, 502285, Telangana, India
 ³Center for Atomistic Modeling and Materials Design, Indian Institute of Technology Madras, Chennai, 600036, Tamil Nadu, India

> *Corresponding author: satyesh@iitm.ac.in Contributing authors: sufyanshk@gmail.com; bsm@iith.ac.in

Abstract

Developing ductile refractory BCC alloys has remained a challenge. The intrinsic ductility (D) of an alloy is the ratio of surface energy (γ_s) and unstable stacking fault energy (γ_{usfe}). Lowering the valence electron concentration has been shown to improve the intrinsic ductility of refractory alloys. However, Re has been widely used to ductilize W, contrary to the low valency criteria suggested in the literature. Here we use density functional theory to calculate the enthalpy of formation, γ_{usfe} and γ_s of Group IV, V, VI elements and their 25 equiatomic binary alloys in BCC crystal structure. We found that positive enthalpy leads to a considerable reduction in γ_{usfe} compared to composition averaged value, resulting in improved intrinsic ductility. Enthalpy is maximum at the equiatomic concentrations indicating the highly repulsive interaction between the alloy constituents and vicer-versa. We found that the repulsive interaction between the alloy constituents leads to a reduction in γ_{usfe} , making alloys intrinsically ductile.

Keywords: stacking fault energy, ductility, high entropy alloys, special quasirandom structures

1 Introduction

The continued cost-pressures and ever stringent environmental norms have pushed aerospace and power generation industries to improve the overall efficiency of their jet-engines and gasturbines [1]. Higher operating temperatures would lead to better thermodynamic efficiency in these propulsion and energy conversion systems [2, 3]. The Ni-based superalloys have ruled this application domain for the past more than six decades [4]. The melting point of the base metal Ni ($T_m=1455^{\circ}$ C) limits the highest operating temperature of these Ni-based superalloys [1, 5]. Alloys based on refractory metals show great potential in this domain due to their high melting-points and their ability to maintain mechanical properties at temperatures higher than the current Ni-based superalloys [5]. Refractory alloys are based on Group IV, V, and VI metals [6–8]. These elements have very high melting-points ($T_m <<1800^{\circ}$ C) and BCC crystal structure which limits their ductility at ambient temperatures.

The lack of deformability at lower temperatures makes refractory alloys difficult to manufacture, which creates a bottleneck in developing them for various applications. Mo has been ductilized by adding 25at.% of Ti/Zr/Hf indicating that alloying with HCP metals should ductilize Mo by reducing the Rice-Thompson parameter [9]. Addition of up to 25at.% of Ta/Re to W has been shown to ductilize it by reducing the overall γ_{usfe} of the alloy[10]. Re addition in 12.5at.% or 25at.% to W has been shown to decrease the shear resistance of $\{110\}<111>$ and $\{112\}<111>$ slip system which in turn improves the ductility of W [11]. Reducing the valence electron concentration (VEC) [6, 12] and reducing the lattice distortion in Nb-based equiatomic BCC alloys has been shown to decrease the Peierls stress which in turn makes alloy deformable [13]. These are few of the refractory alloy ductilizing studies reported in literature. There have been conflicting suggestions about alloying additions to make W deformable. Qian et al. [14] suggests Re addition to W leads to decreased generalized stacking fault energy (γ_{qsfe}) and increased ductility, whereas Ta addition has opposite effect. However, in Qian's work the chemistry of the supercell was W₄₇X (X=Ta or Re), which may not be a true representation of a concenterated alloy. On the contrary, Sheikh et al. [12] suggests alloying with Ti, Zr, Hf, and Re (HCP elements) should ductilize the refractory alloys as it reduces the valence electron concentration (VEC). Similarly, Yang et al. [10] suggests alloying W with Ta or Re should ductilize it by reducing the unstable stacking-fault energy (γ_{usfe}) . None of the previous strategies discuss about the thermodynamic stability of these alloys. This calls for a comprehensive study on the role of various alloying elements on the deformability and thermodynamic stability of refractory alloys.

A general theme in the existing refractory alloy ductilizing studies has been to add low stacking-fault energy (SFE, γ_{sfe}) elements to reduce the overall unstable-SFE (γ_{usfe}) of the alloy, suggesting that the Rule-of-Mixtures (ROM) dictates the overall γ_{usfe} of the alloy. Most of the earlier studies selected alloying elements to get maximum decrease in the overall γ_{usfe} of the alloy, without considering the thermodynamic stability of the alloy. The γ_{usfe} of NiFe [15, 16] and CoCrFeNi [17, 18] calculated using first-principles density functional theory (DFT) matches with their respective experimental value. This shows that the γ_{sfe} can be accurately predicted using DFT. There is a need of a comprehensive study on the effect of alloying elements on the deformability and thermodynamic stability of refractory BCC alloys. Present work addresses these issues using first-principles density functional theory (DFT) simulations. The study gives a strategy to select alloying elements which give

maximum ductilizing effect along with thermodynamic stability of the final alloy.

2 Results and Discussion

To better understand the factors affecting the intrinsic ductility in concentrated BCC alloys, refractory equiatomic binary alloys made from Group-IV (Ti, Zr, Hf), Group-V(V, Nb, Ta), Group-VI(Mo, W), and Group-VII(Re) elements are studied. Atomistic modeling based on DFT provides an accurate description of configurational and chemical space. Based on the binary phase diagrams, not all refractory element combination would be stable as a solid solution in BCC crystal structure. As a first step we take only those combinations which are likely to form a stable BCC solid solution. We show that the enthalpy of formation can be a good estimate of the stability of solid solutions (Section 2.1). Here we report for the first time the influence of enthalpy of formation on intrinsic ductility (D) of alloys. The D is a ratio of unstable stacking-fault energy (γ_{usfe}) and surface energy (γ_s), which has been widely used to compare the intrinsic ductility of refractory alloys [10, 19–21]. However, it needs a reliable calculation of the γ_{usfe} and γ_s .

The γ_{usfe} calculation of solid solutions using DFT, is bound to have errors due to the change in local chemistry while the interface is being sheared and due to the stoichiometry of the shearing interface. The magnitude of this error could alter conclusions, hence an estimate of this error is important while making comparison across alloys. Here we have estimated the maximum error that gets introduced, and discuss ways to minimize it, making our conclusions reliable. The γ_{usfe} of an alloy is strongly influenced by its pure metal constituents. To better understand how pure metal's γ_{usfe} value affect the γ_{usfe} of the alloy, the γ_{usfe} of similar slip systems should be taken into consideration. In present study some of the pure metals have HCP crystal structure and the alloys are considered in BCC structure. Therefore, for both the crystal structures, the γ_{usfe} of equivalent slip system should be considered.

To address these shortcomings which we found in the literature, a DFT-based workflow is developed to calculate lattice parameter (a,c), enthalpy of formation (ΔE_f) , unstable stacking-fault energy (γ_{usfe}) , and surface energy (γ_s) (Figure 1). The workflow is elaborated further in the subsequent sections. The results are shown in the form of heat maps in Figure 2. Additional information can be found in the supplementary file.

2.1 Enthalpy of formation (ΔE_f)

The stability of an alloy (solid solution) is dictated by the Gibbs energy of its constituent phases as,

$$\Delta G = \Delta H - T\Delta S$$

$$= \Delta E_f + \Delta (PV) - T\{\Delta S_{config} + \Delta S_{vib} + \Delta S_{mag} + \Delta S_{elec}\}$$

where ΔE_f is the enthalpy of formation at 0K, $\Delta(PV)$ is the pressure-volume term, ΔS_{config} is the configurational entropy, ΔS_{vib} is the vibrational entropy, ΔS_{mag} is the magnetic entropy, ΔS_{elec} is the electronic entropy. The $\Delta(PV)$ term can be ignored [22]. Therefore the equation becomes,

$$\Delta G = \Delta E_f - T \Delta S_{config} - T \{ \Delta S_{vib} + \Delta S_{mag} + \Delta S_{elec} \}$$

For an equiatomic binary alloy AB, ΔE_f is calculated with the relation [23],

$$\Delta E_f^{AB} = E_{AB} - 0.5 * (E_A + E_B)$$

where E_{AB} is the energy per atom of alloy AB in BCC symmetry, E_A and E_B , are the energy of constituents A and B in their most stable phase. All values are in the units of eV/Atom. The 9 alloying elements form a total of 36 equiatomic binary alloys. Out of these 36 alloys, 6 systems containing both the constituents being HCP, are not considered in the present study. Figure 2a shows the enthalpy of formation (ΔE_f , eV/Atom) values in the form of heat map. We have not considered VRe [24], TaRe [25], HfW [26], ZrW [27], VHf [28], VZr [29], having ΔE_f , -0.2456, -0.1942, 0.1114, 0.1477, 0.1631, 0.1710 meV/Atom respectively, for subsequent analysis as they can either form intermetallic (VRe, TaRe) due to very negative ΔE_f or they can segregate (HfW, ZrW, VHf, VZr) due to very positive ΔE_f . The ΔE_f values of alloy considered ranges from -0.1232eV/Atom (TaMo) to 0.0994eV/Atom (WRe).

The ΔE_f value of 0.0994meV/Atom appear very large for a solid solution to be stable. For an equiatomic binary alloy, the $T\Delta S_{config}$ term has value of about 18 meV/Atom at 300K. Since WRe forms a stable solid solution [30], we expect that the other entropic contributions would be sufficiently large ($\approx 80 \text{meV/Atom}$) to overcome the 0.0994eV/Atom ΔE_f value. Although we take WRe as an extreme case of having the most positive ΔE_f (among the presently considered alloys), depending upon the $T\Delta S_{config}$ and $T\Delta S_{vib}$ values, not all alloys may be stable.

2.2 Unstable stacking-fault energy (γ_{usfe})

Within DFT, the γ_{usfe} is calculated using the relation given below,

$$\gamma_{usfe} = \frac{E_{faulted} - E_{pristine}}{(Area \ of \ Plane)}$$

where the $E_{faulted}$ is the energy of supercell having a stacking fault and the $E_{pristine}$ is the energy of pristine supercell. The $\{110\}$ <111> slip system of BCC metals/alloys has the lowest energy barrier for activation. Therefore, we have chosen the same slip system in present analysis.

2.2.1 Slip system

The γ_{usfe} of an alloy strongly depends on the γ_{usfe} of its constituent pure metals. In order to understand how the γ_{usfe} of pure elements affect the γ_{usfe} of an alloy, comparison of similar similar slip systems should be made. Since some of the pure metal constituents of alloy have HCP crystal structure, the $\{110\}<111>$ slip system of BCC should be compared with an equivalent slip system in HCP crystal structure. The $\{0001\}$ slip plane in HCP crystal structure have similar close-packed arrangement of atoms as that in $\{110\}$ slip plane of BCC crystal structure. The $\{0001\}$ slip plane SFE curves of Zr are shown in Figure 3a for $<11\bar{2}0>$ and in Figure 3c for $<10\bar{1}0>$ slip direction. Figure 3e shows the SFE curve of Nb for $\{110\}<111>$ slip system. From Figures 3b and 3f, it is observed that the atomic arrangements in BCC- $\{110\}$ and HCP- $\{0001\}$ slip planes is similar. Therefore, from Figure 3 it is clear that the $\{110\}<111>$ γ_{usfe} of BCC crystal structure should be compared with the $\{0001\}<11\bar{2}0>$ γ_{usfe} of HCP crystal structure.

2.2.2 Shearing interface stoichiometry

Special quasirandom structures (SQS) have been extensively used to predict the SFE of alloys due to their simplicity in capturing the inherent chemical disorder present in the alloys [31]. In present work, the SQS supercell with in-plane dimensions equal to 4 and 3 times of the first nearest neighbor distance of the BCC symmetry are generated (Figure S1), considering the pair, triplet, and quadruplet with cut-off distance equal to the regular BCC unit cell lattice parameter (2^{nd} nearest neighbor distance). The supercell have 10 planes of (110) type giving 9 shearing interfaces as shown in Figure S1. A vacuum of 10Å is added to the supercell to prevent the interactions due to the periodic boundary condition. To calculate the γ_{usfe} , the atoms in top two planes and bottom two planes are fixed in all directions, whereas, the remaining atoms from the middle six planes are fixed only in slip direction. There are four [111]-type slip directions available for every shearing interface, giving 4 different γ_{usfe} values. Therefore, the same supercell can gives 36 different γ_{usfe} values.

Using the above methodology, we calculated the γ_{usfe} for (110)[111] slip system of WRe alloy (Figure 4). For any shearing interface the energy change in the pristine and slipped supercell is due to the change in the local bonding environment. Out of the 4 possible γ_{usfe} , we choose the one with the minimum difference in energy of pristine and sheared slab as shown in Figure S2 and S3. Therefore there are 9 γ_{usfe} values shown in in Figure 4 instead of 36. As observed from Figure 4, the γ_{usfe} varies from 906 to 1199 mJ/m². Similarly the energy difference between pristine and sheared supercell varies from 0.5 to 109 mJ/m² (lower inset in Figure 4). There are two shearing interfaces in Figure 4 having the same stoichiometry as that of the overall supercell chemistry (WRe). These two shearing interfaces give 1110mJ/m² and 1086mJ/m² γ_{usfe} value. It indicates that the 2nd nearest neighbor also influences the γ_{usfe} . We have taken 1110mJ/m² as the γ_{usfe} value of WRe in present study as this shearing interface was having the lowest energy difference of 1.6mJ/m² between the pristine and sheared supercell.

Based on the above discussion, one should consider only the equiatomic shearing interface. Since the supercell has shearing interfaces that do not have equiatomic stoichiometry, it is assumed that all possible values of γ_{usfe} can exist. The strategy in the literature have been to report an average γ_{usfe} obtained from all shearing interfaces. Such approach does not assure a specific value of error that gets introduced. From WRe results (Figure 4), it clear that stoichiometry strongly affect the γ_{usfe} . That is because of nearest neighbor bond in the shearing interface. Since the intent is to calculate the γ_{usfe} for an equiatomic alloy, we choose the value corresponding to equiatomic shearing interface. Among the two interfaces that have same stoichiometry in Figure 4, there is a difference in γ_{usfe} value due to different set of second nearest neighbors. For the rest of the alloys, the obvious choice of γ_{usfe} will be from the shearing interface having the same stoichiometry as that of the supercell. We found that the maximum energy difference between the pristine and the sheared supercell is 60mJ/m^2 . This error is alloy dependent, whereas the lowest error is 0mJ/m^2 in NbTa. Such error estimation which could affect the interpretation have not been discussed in the literature.

2.2.3 On the origin of γ_{usfe} of binary alloys

Figure 2c shows the γ_{usfe} calculated using First-principles DFT method, in the form of heat map for pure elements and the alloys under study. The HCP elements have the lowest γ_{usfe} except Re. For pure metals, the overall trend is of increasing γ_{usfe} as we move right in the periodic table from Group-IV to Group-VII. W (1773mJ/m³) has the highest γ_{usfe} whereas Zr (457mJ/m³) has the lowest γ_{usfe} . For alloys, the DFT-calculated γ_{usfe} ranges from 454mJ/m² (TaZr) to 1681mJ/m² (MoW). Figure 2d shows the change in γ_{usfe} of the alloys from their composition averaged value ($\Delta \gamma_{usfe}$) as calculated below,

$$\Delta \gamma_{usfe} = \frac{\gamma_{usfe}^{DFT} - \gamma_{usfe}^{ROM}}{\gamma_{usfe}^{ROM}} \times 100$$

The $\Delta \gamma_{usfe}$ ranges from -41% (MoRe) to +20% (MoV). As observed from Figures 2c and Figure 2d, the ROM overestimates the γ_{usfe} for a number of alloys. For example, the DFT-calculated γ_{usfe} for WRe and MoRe is 1110mJ/m² and 889mJ/m² respectively. However the -34% (WRe) and -41% (MoRe) $\Delta \gamma_{usfe}$ indicates that ROM overestimates the γ_{usfe} by a large margin and is not a reliable method to get the correct values. This also suggests that the γ_{usfe} of alloys is dictated by the nature of bonds between the constituent atoms.

The positive and negative $\Delta \gamma_{usfe}$ can be due to the repulsive or attractive interaction between the constituent atoms. One of the parameter to assess the nature of interaction is enthalpy of formation (ΔE_f) . The ΔE_f of equiatomic alloy captures the attractive (negative ΔE_f) or repulsive (positive ΔE_f) interaction between atoms even if the crystal structure of metals that form the alloy are not the same. For example, W and Re have BCC and HCP crystal structure in their pure state, respectively. The ΔE_f of W25-Re75 alloy in BCC crystal structure will have contribution from change in crystal structure of Re from HCP to BCC, apart from the interaction between atoms. In non-equiatomic alloys with different crystal structure of constituents, the ΔE_f does not reflect attractive or repulsive interaction alone, but for alloy with constituent metals in the same crystal structure, ΔE_f of any alloy chemistry will reflect the nature of interaction. Figure 5a shows the $\Delta \gamma_{usfe}$ vs. ΔE_f . A linear fit to the data in Figure 5a has a slope of -2.13 with Pearson's r (correlation parameter) of -0.85. This indicates a strong inverse correlation between ΔE_f with $\Delta \gamma_{usfe}$. The ΔE_f is maximum at equiatomic composition as the number of A-B bonds in an AB alloy would be the highest at equiatomic composition. Inverse correlation between $\Delta \gamma_{usfe}$ and ΔE_f suggests that maximum $\Delta \gamma_{usfe}$ (positive or negative) would occur at equiatomic composition. Figure 5b shows the γ_{usfe} values for NbxV(1-x) (x \in [0,0.25,0.75,1]) alloy. The largest $\Delta\gamma_{usfe}$ occurs at equiatomic concentration (Figure 5b). The present analysis shows many possible alloy combinations which can lead to reduced γ_{usfe} in refractory binary alloys from their average values.

2.3 Surface energy (γ_s)

Similar to γ_{usfe} calculation, the surface energy (γ_s) is calculated for the interface having equiatomic stoichiometry/formula composition. The equiatomic shearing interface of the

supercell is exposed to vacuum of 10Å. The γ_s is calculated using the relation given below,

$$\gamma_s = \frac{E_{with-vacuum} - E_{no-vacuum}}{2 \times (Area\ of\ Plane)}$$

where the $E_{with-vacuum}$ is the energy per atom of the supercell with vacuum and $E_{no-vacuum}$ is the energy per atom of the supercell without vacuum. Figure 2e shows the (110) γ_s calculated using First-principles DFT method, in the form of heat map for pure elements and the alloys under study. For Ti, Zr, Hf, and Re, the γ_s is reported for (0001) plane. The γ_s ranges from 3190mJ/m² (VW) to 1662mJ/m² (NbZr). Figure 2f shows the percentage change in γ_s values of the alloys from their composition averaged values ($\Delta \gamma_s$, calculated similar to $\Delta \gamma_{usfe}$). The $\Delta \gamma_s$ ranges from -20% (MoZr) to 20% (NbRe). Figure 6a shows the $\Delta \gamma_s$ vs. the E_f . A linear fit to the data in Figure 6b has a slope of -0.62 with Pearson's r (correlation parameter) of -0.49. This indicates that the ΔE_f does not strongly influences the γ_s .

2.4 Ductility parameter (D)

Ductility parameter is defined as the ratio of surface energy to unstable stacking fault energy [32, 33].

$$D = \frac{\gamma_s}{\gamma_{usfe}}$$

$$D > 1 \Longrightarrow \gamma_s > \gamma_{usfe} \Longrightarrow \text{Intrinsically Ductile}$$

$$D < 1 \Longrightarrow \gamma_s < \gamma_{usfe} \Longrightarrow \text{Intrinsically Brittle}$$

It quantifies the competition between the energy cost of creating a new crack surface and the energy cost of nucleating new dislocations in the stress field of the crack tip. Recent studies have relied on D to assess the intrinsic ductility of refractory alloys [10, 19–21]. Figure 2b shows the D calculated for pure metals and alloys in the form of heat map. The D ranges from 4.16 (TaTi) to 1.81 (MoW). As discussed in Section 2.2 and 2.3, the ΔE_f influences γ_{usfe} much more strongly than γ_s . Similarly, to understand the relation between ΔE_f and percentage change in D (ΔD , similar to $\Delta \gamma_{usfe}$) from its composition averaged value, we plot ΔD vs. ΔE_f in Figure 6b. A linear fit to the data in Figure 6b has a slope of 1.87 with Pearson's r (correlation parameter) of 0.66. The γ_s does not show any specific relationship with E_f as discussed in Section 2.3. However, the γ_{usfe} shows a strong relationship with E_f as discussed in Section 2.2. This indicates a positive influence of ΔE_f on controlling the D of refractory binary alloys. There is a positive correlation between ΔD and ΔE_f , but it is not as strong as that of γ_{usfe} , since it has contribution from γ_s as well.

The WRe and MoRe has the largest positive ΔD as observed from Figure 6b. Large positive ΔD of Re containing binary alloys is because of large negative $\Delta \gamma_{usfe}$ (Figure 5a) primarily due to repulsive nature of bonds between Re-W and R-Mo atoms; and large negative $\Delta \gamma_s$ (Figure 6a). A positive ΔD is observed for alloy containing Group-IV (Ti, Zr, Hf) elements. The positive ΔD explains large ductility reported in Al/Nb/Mo-Ta-Ti-Zr-Hf-V alloy, its sub-systems [12, 34–38] and NbTaTiZrHf [39, 40]. This could be due to large negative $\Delta \gamma_{usfe}$, although $\Delta \gamma_s$ is not favoring ΔD to be positive. The ductility of alloys containing Ti, Zr, and Hf is attributed to the low VEC (<4.5) [12]. However, VEC

criteria fails to explain the role of higher valency Re addition in improving ductility of W and Mo [9, 11, 41]. The present analysis shows that the enthalpy of formation of alloys gives a fairly reliable idea about deformability of refractory alloys apart from dictating their thermodynamic stability; which can be used as a criteria to design new alloy chemistries with desired ductility.

3 Equations

Not applicable.

4 Tables

Not applicable.

5 Figures

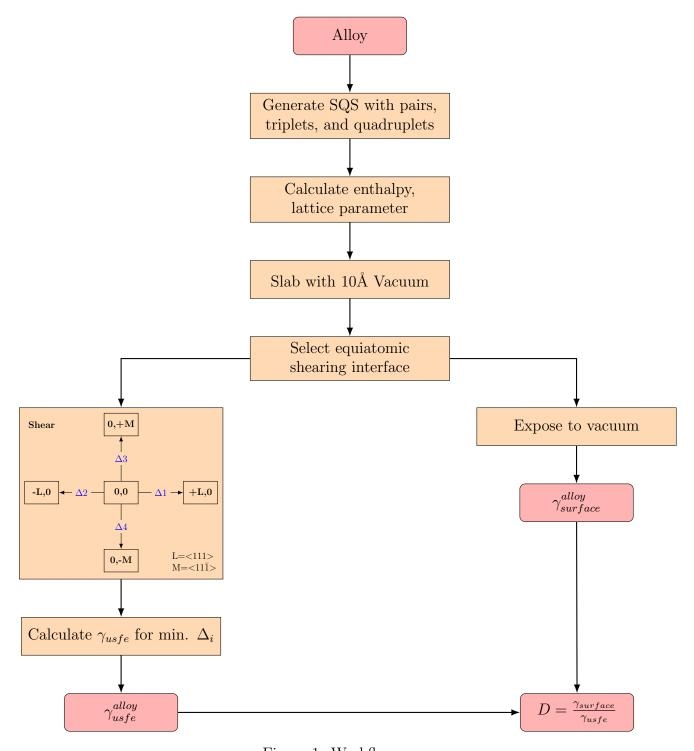


Figure 1: Workflow.

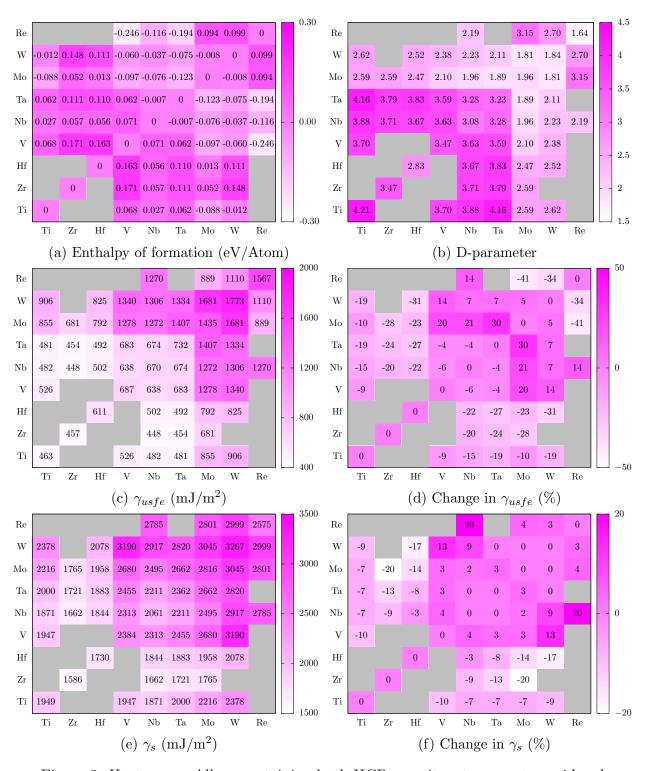


Figure 2: Heat maps. Alloys containing both HCP constituents are not considered.

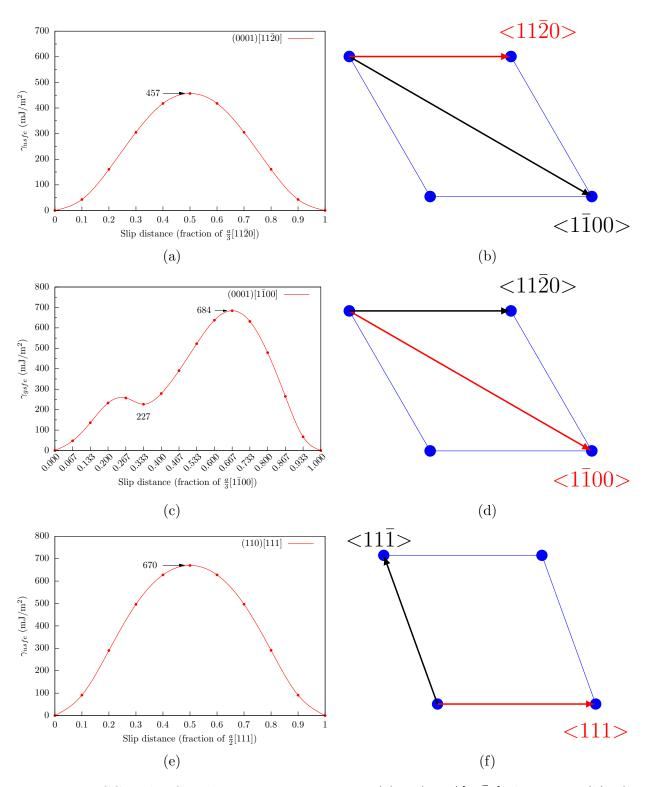


Figure 3: BCC and HCP slip system comparison. (a)Zr $(0001)[11\bar{2}0]$ slip curve, (b)HCP $(0001)[11\bar{2}0]$ slip system projection along [0001] direction, (c)Zr $(0001)[1\bar{1}00]$ slip curve, (d)HCP $(0001)[1\bar{1}00]$ slip system projection along [0001] direction, (e)Nb (110)[111] slip curve, (f)BCC (110)[111] slip system projection along [110] direction. (Out of plane atoms are not shown)

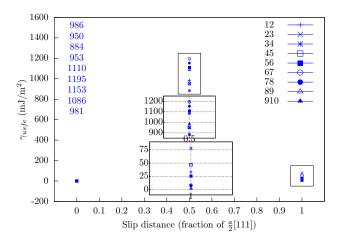


Figure 4: Comparision between γ_{usfe} values calculated for various shearing interfaces from same supercell of WRe. Legend shows the stiochiometry of the shearing interface. Numbers on left shows the γ_{usfe} value. Upper inset shows the range of γ_{usfe} . Lower inset shows the energy difference between before and after one complete slip by $\bar{b} = \frac{a}{2}[111]$.

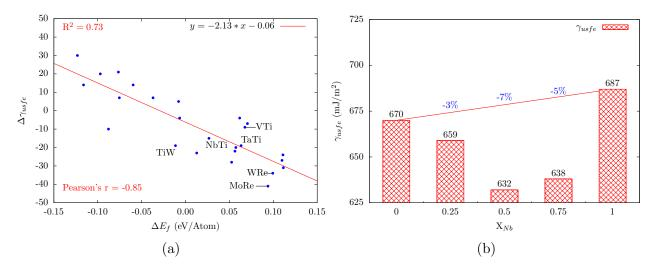


Figure 5: (a)Change in γ_{usfe} as compared to the composition averaged value vs ΔE_f . (b)(110)[111] γ_{usfe} of Nb-V alloys. Numbers in blue show the change in γ_{usfe} from the composition averaged value.

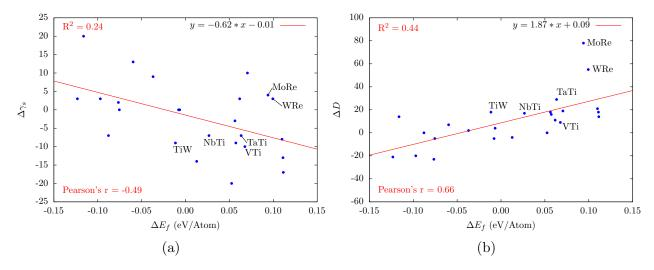


Figure 6: (a) Change in γ_s as compared to the composition averaged value vs ΔE_f . Enthalpy of formation does not affect the γ_s of alloys. (b) Change in intrinsic ductility (D) as compared to the composition averaged value vs ΔE_f . Positive ΔE_f helps improving the deformability of refractory binary alloys.

6 Algorithms, Program codes and Listings

Not applicable.

7 Methods

7.1 Special Quasirandom Structures, Supercell

Special quasirandom structures (SQS) are used to capture chemical disorder in the alloys. SQS are generated using MCSQS code from Alloy Theoretic Automatic Toolkit (ATAT) [42, 43] with pair, triplet, and quadruplet correlations with cut-off distance equal to the BCC unit cell lattice parameter (2^{nd} nearest neighbor distance). The enthalpy of formation (E_f) and lattice parameter are calculated with 128 atoms SQS generated using a BCC unit cell repeated four times each in <100> directions. The experimental values of lattice parameters are taken from Ref.[44]. The reported lattice parameters were within 1% deviation of their experimental values. The supercells were visualized using VESTA software [45].

7.2 First-principles calculations

The first-principles density functional theory (DFT) calculations were performed using Vienna Ab-initio Simulation Package (VASP) with plane-wave basis and projector augmented wave (PAW) pseudopotentials [46–48]. For all calculations, a plane wave kinetic energy cut-off of at least 1.3 times the maximum given in the pseudopotential was used. The electronic exchange-correlation effects were calculated by Perdew-Burke-Erzernhoff generalized gradient approximation (PBE-GGA) [49, 50]. Methfessel-Paxton smearing method with 0.2 eV width was used [51]. Structural relaxation was terminated when the forces on atoms become

less than 1 meV/Å. Tetrahedron method with Blöch correction was used for energy calculation [47]. The Brillouin zone sampling was performed using Monkhorst–Pack [52] scheme with automatically generated mesh with k-point spacing of less than $2\pi \times 0.03$ Å⁻¹.

8 Conclusion

Here we used DFT to calculate the enthalpy of formation (ΔE_f) , unstable stacking-fault energy (γ_{usfe}) , surface energy (γ_s) , and intrinsic ductility (D) of concentrated alloys. We found that the first nearest neighbor has the strongest influence on the γ_{usfe} , hence the shearing interface with formula composition has been chosen for calculating the γ_{usfe} . The calculated γ_{usfe} had maximum error of $\pm 30 \text{mJ/m}^2$. The E_f of the equiatomic binary alloys ranges from -0.25eV/Atom to 0.17eV/Atom. The negative E_f indicates attractive nature of the bonding between the constituents and vice-versa. Here we have shown that the positive ΔE_f shall lead to reduced γ_{usfe} (compared to the composition averaged value) due to the repulsive interaction between the alloy constituents.

Our results suggests that the maximum reduction in γ_{usfe} could be achieved for alloys having positive ΔE_f . Therefore while selecting the alloying elements one should ensure the positive enthalpy of formation is well compensated by the sufficiently large entropy. Our findings provide an explanation for the addition of low valency Ti, Zr, and Hf as well as high valency Re in improving the ductility of refractory alloys. Our findings also explain the failure of empirical rules for increased ductility of refractory BCC alloys where VEC type criterion can be contradictory to experimental observations (e.g. Re addition in W). Taking the effect of enthalpy of formation on the deformability of concentrated alloys is likely to open new directions in the design of refractory alloys for high temperature applications.

9 Declarations

9.1 Funding

We acknowledge the use of the computing resources at High Performance Computing Environment (HPCE), IIT Madras. This work was supported by Ministry of Education (formerly known as Ministry of Human Resource Development), Government of India (grant numbers: SB20210844MMMHRD008277, SB20210824PHMHRD008488, and SB20210993MMMHRD008470).

9.2 Competing interest

The authors declare no competing interests.

9.3 Ethics approval

Not applicable.

9.4 Consent to participate

Not applicable.

9.5 Consent for publication

Not applicable.

9.6 Availability of data and materials

All the data for the study is in the manuscript and in supplementary file.

9.7 Code availability

Not applicable.

9.8 Authors' contributions

S.M.S. and S.K.Y. developed the initial hypothesis. S.M.S. performed the calculations and drafted the initial manuscript. S.M.S., S.K.Y., and B.S.M. together discussed the results. S.K.Y. and B.S.M. supervised the project. All authors contributed to the manuscript writing.

References

- [1] Matt Baker. Defining Pathways for Realizing the Revolutionary Potential of High Entropy Alloys: A TMS Accelerator Study. Tech. rep. Oct. 2021, p. 116. DOI: 10.7449/HEApathways.
- [2] Jien-Wei Yeh. "Recent progress in high-entropy alloys". In: Annales de Chimie Science des Matériaux 31.6 (Dec. 2006), pp. 633–648. ISSN: 09473580. DOI: 10.3166/acsm. 31.633-648.
- [3] B S Murty et al. "13 Applications and future directions". In: *High-Entropy Alloys* (Second Edition). Ed. by B S Murty et al. Second Edi. Elsevier, 2019, pp. 247–257. ISBN: 978-0-12-816067-1. DOI: https://doi.org/10.1016/B978-0-12-816067-1.00013-8.
- [4] Roger C Reed. The Superalloys: Fundamentals and Applications (Google eBook). 2006,
 p. 372. ISBN: 1139458639.
- [5] Oleg N. Senkov et al. "Development and exploration of refractory high entropy alloys—A review". In: *Journal of Materials Research* 33.19 (Oct. 2018), pp. 3092–3128. ISSN: 0884-2914. DOI: 10.1557/jmr.2018.153.
- [6] Sufyan M. Shaikh et al. "CALPHAD and rule-of-mixtures: A comparative study for refractory high entropy alloys". In: *Intermetallics* 127.May (Dec. 2020), p. 106926. ISSN: 09669795. DOI: 10.1016/j.intermet.2020.106926.
- [7] D. B. Miracle. "High entropy alloys as a bold step forward in alloy development". In: Nature Communications 10.1 (2019), pp. 1–3. ISSN: 20411723. DOI: 10.1038/s41467-019-09700-1.
- [8] B S Murty et al. "2 High-entropy alloys: basic concepts". In: *High-Entropy Alloys (Second Edition)*. Ed. by B S Murty et al. Second Edi. Elsevier, 2019, pp. 13–30. ISBN: 978-0-12-816067-1. DOI: https://doi.org/10.1016/B978-0-12-816067-1.00002-3.
- [9] Clint B. Geller et al. "A computational search for ductilizing additives to Mo". In: Scripta Materialia 52.3 (Feb. 2005), pp. 205–210. ISSN: 13596462. DOI: 10.1016/j.scriptamat.2004.09.034.
- [10] Chaoming Yang and Liang Qi. "Ab initio calculations of ideal strength and lattice instability in W-Ta and W-Re alloys". In: *Physical Review B* 97.1 (Jan. 2018), p. 014107. ISSN: 2469-9950. DOI: 10.1103/PhysRevB.97.014107.
- [11] Yu-Hao Li et al. "Transition from ductilizing to hardening in tungsten: The dependence on rhenium distribution". In: *Acta Materialia* 181 (Dec. 2019), pp. 110–123. ISSN: 13596454. DOI: 10.1016/j.actamat.2019.09.035.
- [12] Saad Sheikh et al. "Alloy design for intrinsically ductile refractory high-entropy alloys". In: *Journal of Applied Physics* 120.16 (Oct. 2016), p. 164902. ISSN: 0021-8979. DOI: 10.1063/1.4966659.
- [13] Y. Y. Zhao et al. "A simplified model connecting lattice distortion with friction stress of Nb-based equiatomic high-entropy alloys". In: *Materials Research Letters* 7.8 (2019), pp. 340–346. ISSN: 2166-3831. DOI: 10.1080/21663831.2019.1610105.

- [14] Jing Qian et al. "Effect of alloying elements on stacking fault energy and ductility of tungsten". In: *Journal of Alloys and Compounds* 737 (Mar. 2018), pp. 372–376. ISSN: 09258388. DOI: 10.1016/j.jallcom.2017.12.042.
- [15] Shijun Zhao et al. "Local-environment dependence of stacking fault energies in concentrated solid-solution alloys". In: *npj Computational Materials* 5.1 (Dec. 2019), p. 13. ISSN: 2057-3960. DOI: 10.1038/s41524-019-0150-y.
- [16] A. J. Zaddach et al. "Mechanical Properties and Stacking Fault Energies of NiFeCr-CoMn High-Entropy Alloy". In: JOM 65.12 (Dec. 2013), pp. 1780–1789. ISSN: 1047-4838. DOI: 10.1007/s11837-013-0771-4.
- [17] M. Beyramali Kivy and M. Asle Zaeem. "Generalized stacking fault energies, ductilities, and twinnabilities of CoCrFeNi-based face-centered cubic high entropy alloys". In: Scripta Materialia 139 (Oct. 2017), pp. 83–86. ISSN: 13596462. DOI: 10.1016/j.scriptamat.2017.06.014.
- [18] S.F. Liu et al. "Stacking fault energy of face-centered-cubic high entropy alloys". In: *Intermetallics* 93.August 2017 (Feb. 2018), pp. 269–273. ISSN: 09669795. DOI: 10.1016/j.intermet.2017.10.004.
- [19] Yong-Jie Hu et al. "Screening of generalized stacking fault energies, surface energies and intrinsic ductile potency of refractory multicomponent alloys". In: *Acta Materialia* 210 (May 2021), p. 116800. ISSN: 13596454. DOI: 10.1016/j.actamat.2021.116800.
- [20] O. N. Senkov and D. B. Miracle. "Generalization of intrinsic ductile-to-brittle criteria by Pugh and Pettifor for materials with a cubic crystal structure". In: *Scientific Reports* 11.1 (2021), pp. 10–13. ISSN: 20452322. DOI: 10.1038/s41598-021-83953-z.
- [21] Eleanor Mak, Binglun Yin, and W. A. Curtin. "A ductility criterion for bcc high entropy alloys". In: *Journal of the Mechanics and Physics of Solids* 152.July 2020 (2021), p. 104389. ISSN: 00225096. DOI: 10.1016/j.jmps.2021.104389.
- [22] A. Van de Walle and G. Ceder. "The effect of lattice vibrations on substitutional alloy thermodynamics". In: *Reviews of Modern Physics* 74.1 (2002), pp. 11–45. ISSN: 00346861. DOI: 10.1103/RevModPhys.74.11.
- [23] Dongwon Shin et al. "First-principles study of ternary fcc solution phases from special quasirandom structures". In: *Physical Review B* 76.14 (Oct. 2007), p. 144204. ISSN: 1098-0121. DOI: 10.1103/PhysRevB.76.144204.
- [24] Pierre Villars and Hiroaki Okamoto, eds. Re-V Binary Phase Diagram 0-100 at. {\%} V: Datasheet from "PAULING FILE Multinaries Edition 2012" in SpringerMaterials. DOI: https://materials.springer.com/isp/phase-diagram/docs/c_0902814.
- [25] Pierre Villars and Hiroaki Okamoto, eds. Re-Ta Binary Phase Diagram 0-100 at. {\%} Ta: Datasheet from "PAULING FILE Multinaries Edition 2012" in SpringerMaterials. DOI: https://materials.springer.com/isp/phase-diagram/docs/c_0100260.
- [26] Pierre Villars and Hiroaki Okamoto, eds. Hf-W Binary Phase Diagram 0-100 at. \\%\ W: Datasheet from "PAULING FILE Multinaries Edition 2012" in SpringerMaterials. DOI: https://materials.springer.com/isp/phase-diagram/docs/c_0907545.

- [27] Pierre Villars and Hiroaki Okamoto, eds. W-Zr Binary Phase Diagram 0-100 at. {\%} Zr: Datasheet from "PAULING FILE Multinaries Edition 2012" in SpringerMaterials. DOI: https://materials.springer.com/isp/phase-diagram/docs/c_0904967.
- [28] Pierre Villars and Hiroaki Okamoto, eds. *Hf-V Binary Phase Diagram 0-100 at.* {\%} *V: Datasheet from "PAULING FILE Multinaries Edition 2012" in SpringerMaterials*. DOI: https://materials.springer.com/isp/phase-diagram/docs/c_0100184.
- [29] Pierre Villars and Hiroaki Okamoto, eds. V-Zr Binary Phase Diagram 0-100 at. {\%} Zr: Datasheet from "PAULING FILE Multinaries Edition 2012" in SpringerMaterials. DOI: https://materials.springer.com/isp/phase-diagram/docs/c_0905433.
- [30] Pierre Villars and Hiroaki Okamoto, eds. Re-W Binary Phase Diagram 0-100 at. \\%\ W: Datasheet from "PAULING FILE Multinaries Edition 2012" in SpringerMaterials. DOI: https://materials.springer.com/isp/phase-diagram/docs/c_0904355.
- [31] Alex Zunger et al. "Special quasirandom structures". In: *Physical Review Letters* 65.3 (July 1990), pp. 353–356. ISSN: 0031-9007. DOI: 10.1103/PhysRevLett.65.353.
- [32] James R. Rice. "Dislocation nucleation from a crack tip: An analysis based on the Peierls concept". In: *Journal of the Mechanics and Physics of Solids* 40.2 (Jan. 1992), pp. 239–271. ISSN: 00225096. DOI: 10.1016/S0022-5096(05)80012-2.
- [33] U. V. Waghmare et al. "Effects of alloying on the ductility of MoSi 2 single crystals from first-principles calculations". In: *Modelling and Simulation in Materials Science and Engineering* 6.4 (July 1998), pp. 493–506. ISSN: 0965-0393. DOI: 10.1088/0965-0393/6/4/013.
- [34] B. Schuh et al. "Thermodynamic instability of a nanocrystalline, single-phase TiZrNbHfTa alloy and its impact on the mechanical properties". In: *Acta Materialia* 142 (2018), pp. 201–212. ISSN: 13596454. DOI: 10.1016/j.actamat.2017.09.035.
- [35] Chien Chang Juan et al. "Simultaneously increasing the strength and ductility of a refractory high-entropy alloy via grain refining". In: *Materials Letters* 184 (2016), pp. 200–203. ISSN: 18734979. DOI: 10.1016/j.matlet.2016.08.060.
- [36] S. Y. Chen et al. "Peierls barrier characteristic and anomalous strain hardening provoked by dynamic-strain-aging strengthening in a body-centered-cubic high-entropy alloy". In: *Materials Research Letters* (). DOI: 10.1080/21663831.2019.1658233.
- [37] Luis Casillas-Trujillo et al. "Interstitial carbon in bcc HfNbTiVZr high-entropy alloy from first principles". In: *Physical Review Materials* 4.12 (Dec. 2020), p. 123601. ISSN: 2475-9953. DOI: 10.1103/PhysRevMaterials.4.123601.
- [38] V. Soni et al. "Microstructural Design for Improving Ductility of An Initially Brittle Refractory High Entropy Alloy". In: Scientific Reports 8.1 (2018), pp. 1–10. ISSN: 20452322. DOI: 10.1038/s41598-018-27144-3.
- [39] O.N. Senkov et al. "Microstructure and room temperature properties of a high-entropy TaNbHfZrTi alloy". In: *Journal of Alloys and Compounds* 509.20 (May 2011), pp. 6043–6048. ISSN: 09258388. DOI: 10.1016/j.jallcom.2011.02.171.

- [40] O. N. Senkov and S. L. Semiatin. "Microstructure and properties of a refractory high-entropy alloy after cold working". In: *Journal of Alloys and Compounds* 649 (Nov. 2015), pp. 1110–1123. ISSN: 09258388. DOI: 10.1016/j.jallcom.2015.07.209.
- [41] Chai Ren et al. "Methods for improving ductility of tungsten A review". In: *International Journal of Refractory Metals and Hard Materials* 75.January (2018), pp. 170–183. ISSN: 22133917. DOI: 10.1016/j.ijrmhm.2018.04.012.
- [42] A. van de Walle, M Asta, and G. Ceder. "The Alloy Theoretic Automated Toolkit: A User Guide". In: *Calphad* 26.4 (Dec. 2002), pp. 539–553. ISSN: 03645916. DOI: 10. 1016/S0364-5916(02)80006-2.
- [43] A. Van De Walle et al. "Efficient stochastic generation of special quasirandom structures". In: Calphad: Computer Coupling of Phase Diagrams and Thermochemistry 42 (2013), pp. 13–18. ISSN: 03645916. DOI: 10.1016/j.calphad.2013.06.006.
- [44] Yibin Xu, Masayoshi Yamazaki, and Pierre Villars. "Inorganic materials database for exploring the nature of material". In: *Japanese Journal of Applied Physics* 50.11 PART 2 (2011). ISSN: 00214922. DOI: 10.1143/JJAP.50.11RH02.
- [45] Koichi Momma and Fujio Izumi. "VESTA 3 for three-dimensional visualization of crystal, volumetric and morphology data". In: *Journal of Applied Crystallography* 44.6 (Dec. 2011), pp. 1272–1276. ISSN: 0021-8898. DOI: 10.1107/S0021889811038970.
- [46] G. Kresse and J. Hafner. "Ab initio molecular dynamics for liquid metals". In: *Physical Review B* 47.1 (1993), pp. 558–561. ISSN: 01631829. DOI: 10.1103/PhysRevB.47.558.
- [47] P. E. Blöchl. "Projector augmented-wave method". In: *Physical Review B* 50.24 (1994), pp. 17953–17979. ISSN: 01631829. DOI: 10.1103/PhysRevB.50.17953.
- [48] G Kresse and J Furthmüller. "Efficient iterative schemes for ab initio total-energy calculations using a plane-wave basis set". In: *Physical Review B* 54.16 (Oct. 1996), pp. 11169–11186. DOI: 10.1103/PhysRevB.54.11169.
- [49] John P. Perdew, Kieron Burke, and Matthias Ernzerhof. "Generalized gradient approximation made simple". In: *Physical Review Letters* 77.18 (1996), pp. 3865–3868. ISSN: 10797114. DOI: 10.1103/PhysRevLett.77.3865.
- [50] D. Joubert. "From ultrasoft pseudopotentials to the projector augmented-wave method". In: *Physical Review B Condensed Matter and Materials Physics* 59.3 (1999), pp. 1758–1775. ISSN: 1550235X. DOI: 10.1103/PhysRevB.59.1758.
- [51] M. Methfessel and A. T. Paxton. "High-precision sampling for Brillouin-zone integration in metals". In: *Physical Review B* 40.6 (1989), pp. 3616–3621. ISSN: 01631829. DOI: 10.1103/PhysRevB.40.3616.
- [52] Hendrik J. Monkhorst and James D. Pack. "Special points for Brillouin-zone integrations". In: *Physical Review B* 13.12 (June 1976), pp. 5188–5192. ISSN: 0556-2805. DOI: 10.1103/PhysRevB.13.5188.